Measuring seeing with a Shack–Hartmann wave-front sensor during an active-optics experiment

Yong Zhang, Dehua Yang, and Xiangqun Cui

We describe the measurement of atmospheric enclosure seeing along a 120-m light path by use of a Shack–Hartmann wave-front sensor (S-H WFS) for the first time to our knowledge in the Large Sky Area Multi-Object Fiber Spectroscopic Telescope (LAMOST) outdoor active-optics experiment system, based on the differential image motion method and a S-H WFS. Seeing estimates that were gained with the S-H WFS were analyzed and found to be in close agreement with the actual seeing conditions, the estimates of refractive-index structure constant, and the thin-mirror active optics results, which usually include the shape sensing precision and the active correction precision of the experimental system. Finally, some countermeasures against poor seeing conditions were considered and adopted. © 2004 Optical Society of America

OCIS codes: 010.1330, 010.7350.

1. Introduction

The performance of large telescopes is highly dependent on image quality and good seeing conditions, which has become increasingly important. Traditionally, astronomers have relied on measuring image quality with small telescopes and differential image motion monitors, which are well understood now. Image quality is directly related to perturbations of the incoming wave front. Light propagating through the atmosphere suffers random aberrations as it passes through regions where there is turbulent mixing of air of different temperatures and hence of different refractive indices. With wave-front sensing methods, wave-front fluctuations can be directly analyzed to provide quantitative information on seeing conditions independently of what telescope is used.

The Large Sky Area Multi-Object Fiber Spectroscopic Telescope (LAMOST) is a meridian reflecting ground-based Schmidt telescope with its optical axis fixed in the meridian plane. It consists of a reflecting Schmidt corrector at the northern end, a spherical primary mirror at the southern end, and a focal plane between. The LAMOST, which combines both thin mirror and segmented mirror active optics, controls not only aspherical shape to correct spherical aberration of the primary mirror but also the cofocus of all 24 submirrors. To prepare for real application and to optimize the design of the LAMOST, an outdoor experiment with full-scale but unit optical components was started in the spring of 2001 in Nanjing. We expect to get some results to enable us to make decisions for the specification and design of the LAMOST from this system. A Shack–Hartmann wave-front sensor (S-H WFS) is mounted on the focal platform to test the shape of the Schmidt plate corrector in our LAMOST outdoor active optics experiment. Enclosure seeing here is difficult because of the long light path near the ground, and dome seeing is of little significance. The correcting precision of the thin mirror active optics is greatly influenced by seeing. So, following the design of the Differential Image Motion Monitor (DIMM), one of the present authors (Cui) suggested developing the technology to measure seeing by using the S-H WFS. This technology began as a by-product of a LAMOST active-optics experiment at first but is now an essential part of the experimental program.

The theory of S-H WFS and seeing measurement is reviewed below. Seeing estimates and statistics obtained with this instrument are compared with actual site conditions and with the precision of an active-optics experiment.

The authors are with the National Astronomical Observatories, Nanjing Institute of Astronomical Optics and Technology, No. 188 Bancang Street, Chinese Academy of Sciences, Nanjing 210042, China. Y. Zhang's e-mail address is yzh@mail.nairc.ac.cn.

Received 22 June 2003; revised manuscript received 8 October 2003; accepted 22 October 2003.
0003-6935/04/040729-06$15.00/0

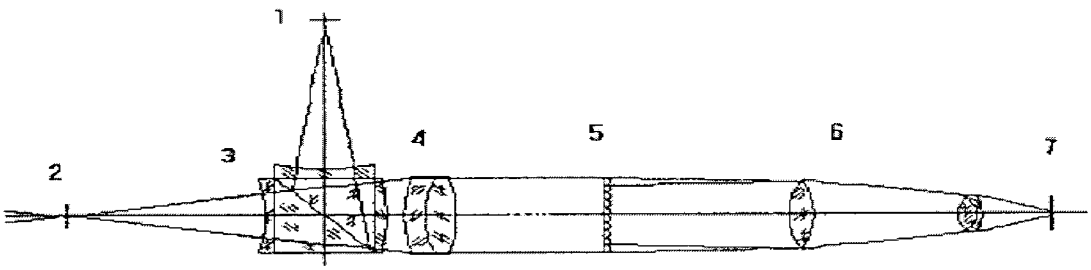

Fig. 1. Schematic configuration of the S-H optical system: 1, reference source; 2, focus to be tested; 3, beam-splitter cube; 4, collimator; 5, lenslet array; 6, reduction system; 7, CCD target.

2. Theory

The S-H wave-front test has been widely used in optical shop testing and in telescopes, especially in active optics and adaptive optics. But it is not well known in the field of seeing measurement. The measurement data of the S-H test are the coordinate differences of the S-H grid that contain information on wave-front slope. Therefore a numerical reconstruction is necessary for integrating these slope data to produce the desired the wave-front contour map.

The S-H WFS is shown schematically in Fig. 1.[1] A beam of light from reference point 1 passes through a beam-splitter cube, a collimator, and a lenslet array and then forms the S-H grid array, which is imaged onto the CCD focal plane by a reducing system. This spot array on the CCD is used as the S-H standard grid array. Another beam of light from the optical system to be measured passes the same way and alternately with the first beam, and both are imaged onto the CCD as the real grid array. By measuring the position differences between two sets of spots, one can reconstruct the real wave front by using integrals, and other applications such as seeing measurement can be carried out too. Figure 2(a) shows the original, classical S-H WFS optical model. The wave front that is analyzed is sampled by a lenslet array, leading to almost plane sub-wave-fronts. The focal spot at the focus of each lenslet is then translated laterally, proportionally to the slope of the associated sub-wave-front. In this model the assumption is that each lenslet is independent of the adjacent lenslets. So the model is limited to using lenslet arrays with low *f*-numbers. Figure 2(b) is the sampled wave-front image in the LAMOST active-optics experiment system.

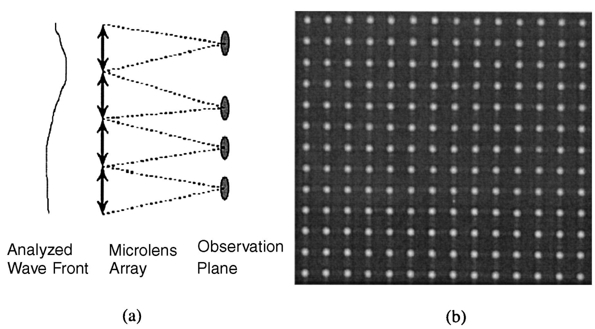

Fig. 2. (a) Classic S-H WFS optical model and (b) the image (part) sampled by our S-H WFS.

As we know, the DIMM operates by measuring the variance of the differential centroid motion for images of a star produced separately from two apertures of known separation within the entrance pupil of a telescope. The differential image motion is unaffected by tracking errors, telescope vibration, or small focus errors and so gives an unbiased estimate of the image degradation that is due to the free atmosphere alone. The standard model for astronomical seeing, developed largely by Tatarski[2] and Fried,[3] is based on the work of Kolmogorov[4] on atmospheric turbulence.[3] As we know, the full width at half-maximum (FWHM) of seeing is the most important factor in the quality of a wave that has propagated through atmospheric turbulence. The DIMM measures the strength of the aberrations that are due to atmospheric turbulence and then predicts the seeing FWHM for a large telescope, assuming the standard seeing model. The aberration strength is parameterized by Fried's parameter (r_0). Small values of r_0 indicate strong turbulence and hence poor seeing.

In terms of our seeing measurement, the lenslet array in the S-H WFS can be and has already been regarded as a Hartmann light-diaphragm array. Our system with any pair of diaphragms is a simple DIMM. That is to say, the DIMM is just our system's special case with only two diaphragms. Because of this one-up design, the superiority of our system obviously lies in the fact that highly accurate, detailed, and reasonably smooth seeing estimates can be obtained if more than one pair of light diaphragms from the lenslet array is chosen, which means that we have more DIMMs and will get more-elaborate seeing results at the same time.

Next, we briefly review the theory of our DIMM[5]: For Kolmogorov turbulence at the near-field approximation, over a distance d the approximate expression for the variance σ_l^2 of the longitudinal motion for $d \geq D$ is given by

$$\sigma_l^2 = 2\lambda^2 r_0^{-5/3}[0.179D^{-1/3} - 0.0968d^{-1/3}], \quad (1)$$

and for the variance σ_t^2 of the transverse motion for $d \geq D$ it is

$$\sigma_t^2 = 2\lambda^2 r_0^{-5/3}[0.179D^{-1/3} - 0.145d^{-1/3}], \quad (2)$$

where r_0 is Fried's[2] seeing parameter, which is a measure of the strength of the seeing distortions. The transverse covariance is exactly 1.5 times larger than the longitudinal covariance, and both decrease as the $-1/3$rd power of the separation.

These variances can be expressed in terms of the total variance for two-dimensional motion through a single aperture of diameter D:

$$\sigma^2 = 0.358(\lambda/r_0)^{5/3}(\lambda/D)^{1/3}, \tag{3}$$

$$r_{0l} = \left[\frac{2\lambda^2(0.179D^{-1/3} - 0.0968d^{-1/3})}{{\sigma_l}^2}\right]^{3/5}, \tag{4}$$

$$r_{0t} = \left[\frac{2\lambda^2(0.179D^{-1/3} - 0.145d^{-1/3})}{{\sigma_t}^2}\right]^{3/5}, \tag{5}$$

$$\mathrm{FWHM} = 0.98(\lambda/r_0). \tag{6}$$

Because r_0 scales as $\lambda^{6/5}$, the image FWHM has only a weak $\lambda^{-1/5}$ dependence on wavelength. For the theoretical Kolmogorov–Tatarski structure function, seeing distortions of the wave front extend to infinitely large spatial scales. Temperature inhomogeneities are responsible for local variations in the refractive index that perturb the otherwise homogeneous propagation of incident light waves. The parameter that describes the turbulent atmosphere, which gives a measure of the intensity of the optical turbulence as it relates to the index inhomogeneities, is the refractive-index structure constant ${C_N}^2$. It is complicated to describe the relationship between ${C_N}^2$ and seeing of the isolated atmosphere in an enclosure near the ground. In our system we can estimate seeing by summing atmosphere seeing and enclosure seeing in a real observing mode. Whereas in the self-collimation mode the optical path is near the local ground, ${C_N}^2$ is usually independent of altitude, and there are spatial and temporal variations along the path. So seeing here is just enclosure seeing along a 120-m folded light path, which is different from the path in a real observing mode. According to temperature $T(r)$ measured by temperature sensors separated by a distance Δr of 1 m, temperature structure constant ${C_T}^2$ and refractive-index structure constant ${C_N}^2$ are easily estimated from the expressions

$${C_T}^2(r) = \frac{\langle[T(r) - T(r + \Delta r)]^2\rangle}{\Delta r^{2/3}}, \tag{7}$$

$${C_N}^2 = \left(77.6 \times 10^{-9}\,\frac{P}{T^2}\right)^2 {C_T}^2, \tag{8}$$

where P is the pressure in millibars and T is the temperature in degrees Kelvin. Through the experiments we also get ${C_T}^2$ and ${C_N}^2$.

3. Description of the System

Figure 3 shows an overview of the LAMOST active-optics experiment system.[6] The point light comes from the S-H WFS onto spherical mirror MB, is reflected to a parallel light, is reflected by plate MA and then converges to a S-H wave-front sensor. In this experimental system the light path is 120 m in a self-collimation closed-loop correction mode, which is double the distance in the LAMOST real observing mode. The light path is only about ~6 m above ground and is surrounded by many trees and high buildings, which cause serious air disturbances and bad enclosure seeing, and they have key influences on the success of our active-optics experiment, which requires great precision.

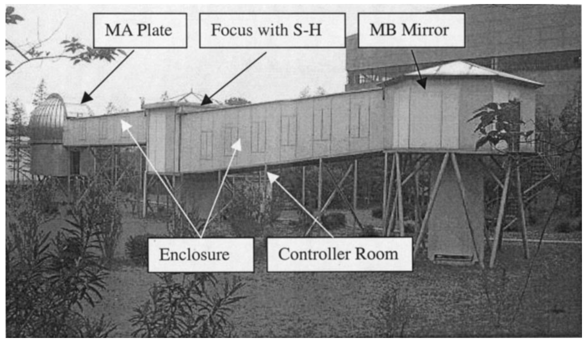

Fig. 3. Overview of the LAMOST outdoor experiment system. MA, reflecting Schmidt corrector of our LAMOST experiment; MB, spherical primary mirror.

In our experimental system, systemic structural and processing parameters of the S-H wave-front sensor are as follows:

- The 1-pixel angular size is 2.183 arc sec;
- The CCD pixel size is 8.6 μm $\times$ 8.3 μm;
- The lenslet subaperture diameter is 0.768 mm, and its corresponding aperture diameter on the entrance pupil (at the Schmidt reflecting corrector plate) is 3.612 cm;
- The lenslet array size is 32 $\times$ 32;
- The reducing ratio is -5.2252;
- There is a sufficiently strong light source, which depends on the controllable voltage;
- The exposure time (one frame period) is 40 ms (a frame rate of 25 Hz);
- The frame size (image resolution) is 552 $\times$ 552;
- The threshold depends on the brightness and contrast of CCD image sampling and is optimized during the process of image spotting.
- The number of sampling frames is 500;
- The wavelength of light is 550 nm; and
- The systemic focal length is 20 m (the same as that of the LAMOST).

Seeing should be calculated at the entrance pupil, that is to say, at the position of the reflecting Schmidt plate. According to Eqs. (4)–(6), two Fried parameters r_0 and their FWHM values can be calculated easily. During our active-optics experiment, three pairs of r_0 are selected, and our final seeing is given by averaging. (Ideally we should choose as many pairs as we can to describe the seeing distribution of the whole enclosure section, but a highly accurate

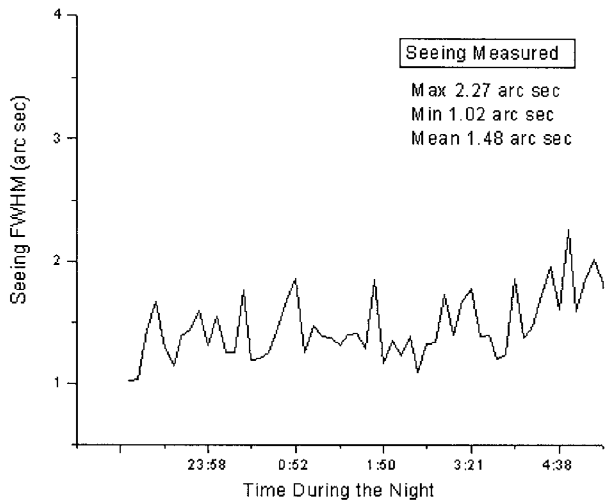

Fig. 4. Distribution of seeing FWHM measured with the S-H WFS on the night of 19–20 December 2002. The mean value is 1.4997 arc sec.

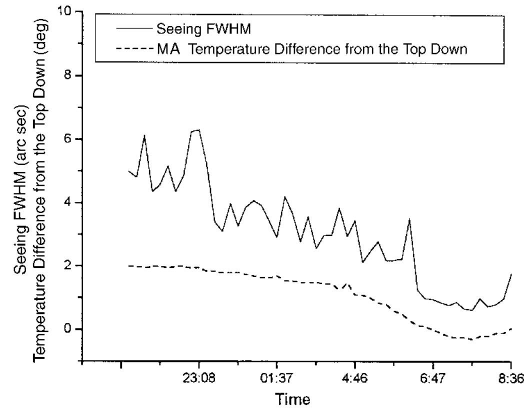

Fig. 5. Distribution of seeing FWHM on the night of 30 November–1 December 2002. The mean value is 3.039 arc sec. The corresponding distribution of temperature difference is given too. MA, reflecting Schmidt corrector of our LAMOST experiment.

result entails the use of a significant amount of computing time). Three pairs cover almost the total field and can express the seeing conditions of the whole system accurately. Enclosure seeing is the most important factor in our active-optics experiment, and there are many temperature sensors to keep tracking the real-time three-dimensional thermal field and C_N^2 variations of the enclosure. Because there is almost solely enclosure seeing in the self-collimation mode, we can gain C_N^2 by using Eqs. (7) and (8) and finding some linear relation between enclosure seeing r_0 and enclosure C_N^2.

4. Experimental Results

During the nights of our active-optics experiments, seeing and temperature measurements are taken at any desired time. Accompanied by the advancement of our active-optics experiments, many useful results have been gained in self-collimation mode. In this mode, most of the seeing is enclosure seeing, and it is easy to analyze the enclosure conditions, which are different from those in tracking mode. Figure 4 shows measured seeing results on the night of 19–20 December 2002. It was rainy on that night. Figure 5 shows another set of seeing results and temperature changes for the night of 30 November–1 December 2002. The sky was clear on that night. The range of seeing results is 1–2 arc sec. From Fig. 5, it is easy to see that seeing is highly correlated with temperature and weather conditions. Figure 6 shows the corresponding estimated mean, which is averaged over the light path of refractive-index structure constant C_N^2. Through our experiments we found that seeing FWHM declines following decreasing temperature difference and vice versa. If it is cloudy or even rainy, good seeing is available. Therefore weather forecasts might be used to predict seeing conditions and help us to arrange our experiment schedule. Furthermore, from Figs. 5 and 6, the seeing FWHM values and the mean of C_N^2 have the same trend of decrease and increase. There is a certain relationship between them. As we know, the seeing FWHM decreases theoretically as 3/5ths of the power of the integral of C_N^2. There is excellent agreement. For further spatial and temporal details on C_N^2, more temperature sensors should be placed along the light path for more-detailed values of C_T^2 in the enclosure.

Measuring with the S-H WFS, we calculate each seeing FWHM from one pair of lenslets, the same as for one DIMM, and it represents only the turbulence conditions of some local part of the total exit pupil plane. The random seeing FWHM has a statistically normal distribution, which can be expressed in terms of its mean value and of its rms value. Here we just choose the seeing FWHM values of the three pairs of lenslets from 23 July 2002 shown in Fig. 7. Their mean values are 1.72, 1.66, and 1.78 arc sec, and their rms values are 0.31, 0.37, and 0.32 arc sec, respectively. The difference of the mean and the rms values of these lenslets pairs is small and therefore is not important.

Figure 8 shows the experimental statistical rela-

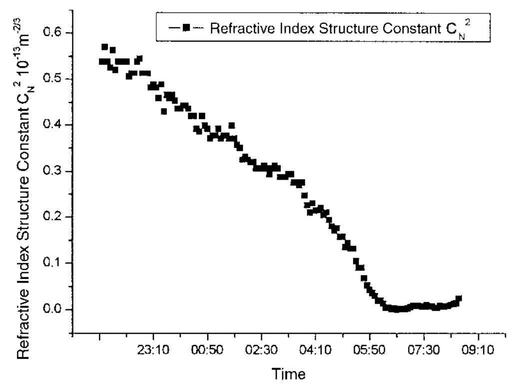

Fig. 6. Mean of the refractive-index structure constant C_N^2 on 30 November–1 December 2002, corresponding to the seeing result in Fig. 5.

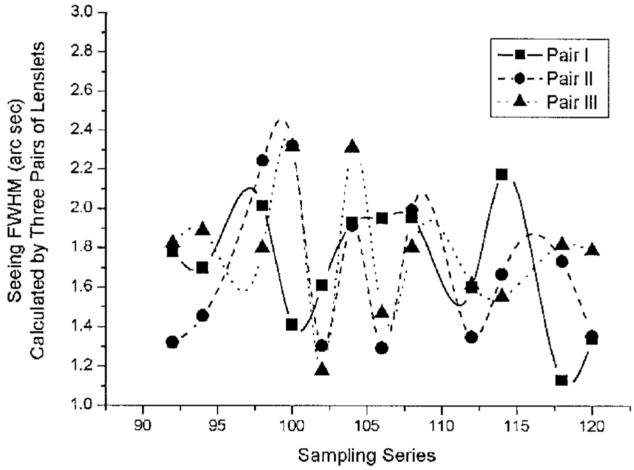

Fig. 7. Seeing FWHM from three pairs of lenslets. Estimates from these three pairs show little difference.

tionship between seeing FWHM and centroid orientation precision. As we know, seeing has a great effect on the precision of our active-optics experiment, especially in our closed loop of thin-mirror active-optics correction. Indoor experiments proved that a high precision of 1/30 pixel can be achieved without causing a seeing problem, whereas in our LAMOST outdoor experiment system it deteriorates to 1/10 pixel and the corresponding wave-front rms reaches almost 0.1 μm. Although this precision includes the image sampling error, processing algorithmic error, and some other random errors and these systemic errors are not introduced by seeing, they are greatly influenced by it. The worse the seeing, the greater the errors. Through the optimizations of a number of sampling frames, threshold, image luminosity, image contrast, and image spot size, a final optimal result is as fitted in Fig. 8. When the seeing FWHM

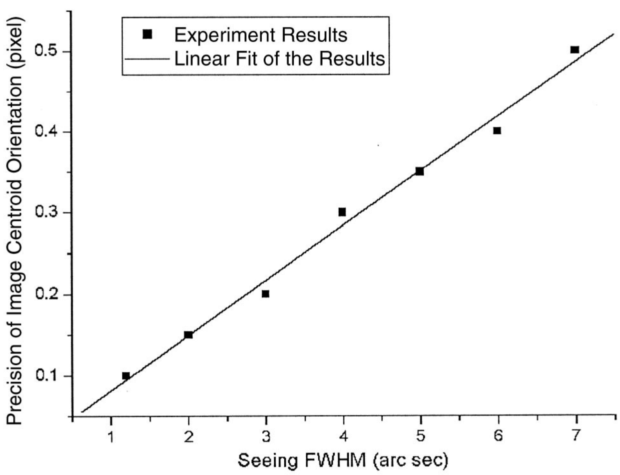

Fig. 8. Statistical linear relationship between precision of image centroid orientation and seeing FWHM in the LAMOST outdoor experimental system.

is below 1.2 arc sec, the precision is not more than 0.1 pixel, mostly because of systematic errors.

The S-H seeing FWHM prediction assumes that the spatial spectrum of wave-front aberrations is well described by the Tatarski structure function. The accuracy of the seeing estimates therefore depends on the validity of the Kolmogorov turbulence model for the spatial scales of interest. According to their results, the S-H sensor will overestimate seeing disc r_0 (underestimate the FWHM) because of the high d/D ratio and the smoothness of seeing of the full aperture as determined by averaging.

5. Conclusions

Controlling and improving seeing is extremely important for working with telescopes. Our goal is to estimate the poor seeing conditions and image quality of our already existing system, to find how they influence the active-optics sensing precision and the wave-front correction precision, and then to find some measures to improve the seeing. Clearly the goal has been achieved now with our S-H WFS.

We have compared measurements made with the DIMM and some other measurements with our S-H WFS findings. The DIMM is just a site survey instrument, whereas the S-H WFS is a wave-front sensing instrument. In seeing measurement, the S-H WFS can be used not only in little telescopes but also in large telescopes, enclosures, and domes to measure all kinds of seeing, whereas the DIMM is used only for stars, mainly to measure atmospheric seeing. Because our sampling time and integral time are much longer than those of the DIMM for correcting the low-frequency figure errors in the Schmidt plate of the LAMOST, our seeing FWHM results from the S-H WFS are similar, whereas the computational time is much longer in our case. The difference between the seeing estimates measured the by S-H WFS and that from the DIMM while both are tracking the same star can be attributed to enclosure-, dome-, and system-induced additional seeing or optical aberrations. We use the experimental seeing and positioning precision relationship to predict seeing, to guide our experimental scheduling, and furthermore to optimize the design of the LAMOST enclosure and of thermal field control. Here we have given the enclosure-seeing results from the S-H WFS, as the DIMM cannot measure enclosure seeing directly. Further atmosphere seeing measurements will be carried out after our active-optics real-tracking experiments begin. If our CCD detector is replaced with an intensified CCD to produce a high frame rate, we will gain more real-time seeing results for the coming LAMOST adaptive-optics experiment.

Now measures have been taken to improve the thermal and seeing conditions of the enclosure; for example, the whole system has been made strictly windproof to maintain the uniformity of the inside atmosphere in a tunnel made from an insulated steel plate with fans and air conditioning added for ventilation,[7] and we even measure real-time temperatures to monitor their changes at many different positions in the light routine at the same time. Qualitative relations from both seeing and environmental temperature are found and used to explain the seeing conditions and to predict the corresponding experimental precision. Further analyses of temperature control and optimization of the enclosure are being made.

References

1. W. Zou and Z. Zhang, "Generalized wave-front reconstruction algorithm applied in a Shack–Hartmann test," Appl. Opt. **39,** 250–268 (2000).
2. V. I. Tatarski, *Wave Propagation in a Turbulent Medium* (McGraw-Hill, New York, 1961).
3. D. L. Fried, "Optical resolution through a randomly inhomogeneous medium for very long and very short exposures," J. Opt. Soc. Am. **56,** 1372–1379 (1966).
4. A. N. Kolmogorov, "The local structure of turbulence in incompressible viscous fluid for very large Reynolds numbers," Dokl. Akad. Nauk. USSR. **30,** 301–305 (1941).
5. M. Sarazin and F. Roddier, "The ESO differential image motion monitor," Astron. Astrophys. **227,** 294–300 (1990).
6. H. Su and X. Cui, "LAMOST project and its current status," in *Large Ground-Based Telescopes*, J. M. Uschmann and L. M. Stepp, eds., Proc. SPIE **4837,** 26–35 (2003).
7. Z. Yao, W. Hao, and F. Zhou, "Dome seeing improvement of LAMOST enclosure," in *Large Ground-Based Telescopes*, J. M. Uschmann and L. M. Stepp, eds., Proc. SPIE **4837,** 198–205 (2003).